Springer

KSME

Journal of Mechanical Science and Technology 24 (4) (2010) 943~949
www.springerlink.com/content/1738-494x
DOI 10.1007/s12206-010-0203-0

Exploiting the orbital motion of water particles for energy extraction from waves †

M. Rafiuddin Ahmed[1], Mohammed Faizal[1], Krishnil Prasad[1], Young-Jin Cho[2], Chang-Goo Kim[2] and Young-Ho Lee[2,*]

[1]*Division of Mechanical Engineering, The University of the South Pacific, Laucala Campus, Suva, Fiji*
[2]*Division of Mechanical and Information Engineering, Korea Maritime University, 1 Dongsam-dong Youngdo-Ku, Busan 606-791, Korea*

(Manuscript Received November 26, 2008; Revised November 13, 2009; Accepted December 31, 2009)

Abstract

In wave motion, the water particles are known to follow orbital paths. This orbital motion was used to drive five-bladed Savonius rotors. Experiments were performed on an array of four rotors placed in a two-dimensional (2-D) wave channel. The flow around the rotors was documented using particle image velocimetry measurements. The submergence of the rotors and the distance between them were varied, and the rotational speeds of the rotors (N_n) were recorded at different wave frequencies. It was found that rotational speeds increased with an increase in the wave frequency, as it amplified the wave height that increased the kinetic energy of the particles in their orbital motion. The rotational speeds decreased when the distance between the rotors increased. High rotational speeds are recorded when the array of the rotors is placed close to the water surface at the smallest centre-to-centre distance between the rotors.

Keywords: Wave energy; Orbital motion; Savonius rotor; Particle image velocimetry; Flow characteristics

1. Introduction

As long as there is wind blowing over the ocean, water waves are always present on the ocean surface, thus offering an infinite source of wave energy [1]. The power that flows in the waves is up to five times greater than the wind that generates the waves, making wave energy more persistent than wind energy [2]. Water wave motions are complex and irregular on the ocean surface. Mathematical analysis can only be utilized for idealized conditions, while experimental studies can be performed on two-dimensional (2-D) waves in channels with parallel side walls. Regular sinusoidal waves [1-5] are easier to study than non-linear waves. The effects of the boundary layer are very small and can be neglected [6]. The common parameters of a sinusoidal wave are the wave period, wavelength, and wave height. Modern instrumentation has allowed for accurate measurements of wave parameters [7, 8]. Particle image velocimetry (PIV) is a standard optical method for instantaneous mapping of flow fields, and it can measure particle velocities over a large 2-D area of a flow field [9]. Most other conventional techniques are intrusive and disturb the flow.

The motion of the waves sets the water particles in orbital motion. A water wave has both longitudinal and transverse motions. In a longitudinal motion, the particles oscillate back and forth parallel to the direction of wave propagation. In a transverse motion, the particles oscillate up and down in their positions [3, 4]. These two motions combine to provide the overall orbital motion. As the waves are formed, the surface water particles rise and move forward with the crest. When the crest passes, particles slow down and fall during the forward motion. When the trough advances, particles slow down their falling rate and move backward. When the trough passes, particles slow down their backward speed and start to rise and move forward with the crest [10]. These movements of water particles result from the longitudinal and transverse oscillations and create the orbital path. The orbital motion of particles is present in deep water waves (depth, $D > \lambda/2$) as well as in shallow water waves ($D < \lambda/20$). However, while the orbit is circular in deep water waves, it is elliptical in shallow water waves, with the major axis in the horizontal direction [2-5]. The motions of the particles are shown in Fig. 1. The radius of the circular orbits in deep water decreases with the increase in depth and ceases at $z < -\lambda/2$. In shallow water, the length of the minor axis decreases with the increase in depth, while that of the major axis remains constant until the bottom; which means that the effect of waves is felt to the bottom [2-5]. In the case when $\lambda/20 < D < \lambda/2$, the waves are called intermediate depth waves.

Surface water waves have energy associated with them, including the kinetic energy of the moving particles and the

† This paper was recommended for publication in revised form by Associate Editor Won-Gu Joo

*Corresponding author. Tel.: +82 51 410 4293, Fax.: +82 51 403 0381
E-mail address: lyh@hhu.ac.kr

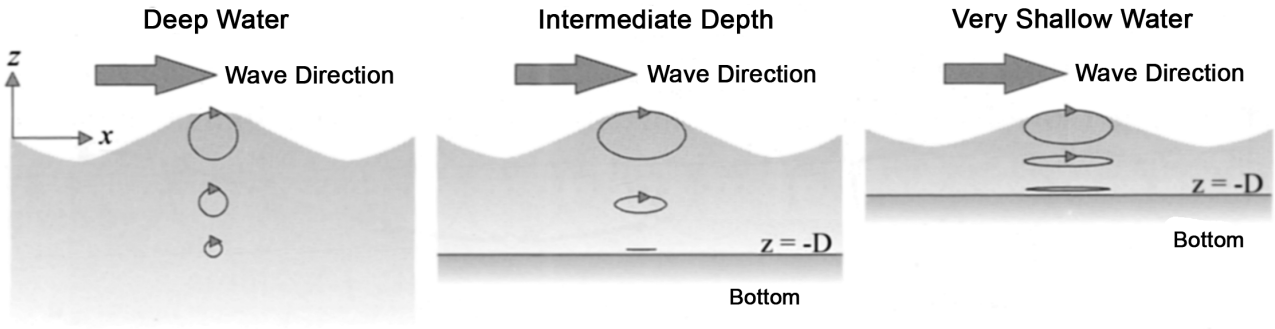

Fig. 1. The orbital motion in deep water, intermediate-depth water, and shallow water waves [4].

potential energy due to the vertical position of water from the mean level. The total energy is proportional to the square of the wave height and is equally divided between kinetic and potential energies [2-5]. A higher wave will have more potential and kinetic energies [11]. A number of devices have been developed to extract energy from waves [2, 3, 12]. Wave energy is currently attracting much attention, as it is available 90% of the time at a given site compared with solar and wind energies, which are available only 20-30% of the time [13].

1.1 Savonius rotors

The Savonius rotor spins due to the differential drag on the curved surfaces [14]. Savonius rotors develop high torque at low rotational speeds but have a low power coefficient [15]. Ocean currents can be used to drive vertical axis Savonius rotors submerged deep in water. The geometry of the blades is such that any flow of water will produce a positive force on the rotor. The rotors depend on the force of the current on the blades to create torque [16].

Savonius rotors have also been used in an attempt to extract wave energy. S. J. Savonius obtained power by using rotors with their axis horizontal and perpendicular to the direction of wave propagation [17]. The kinetic energy of the orbital motion of the water particles can be used to drive water wheels [3] or small Savonius rotors [18]. A number of rotors can be mounted in an array, with their axis horizontal and normal to the direction of wave propagation. If requited, there can be multiple arrays of Savonius rotors. To extract maximum energy, the rotors should be placed close to the free surface, where most of the energy is available. The kinetic energy of the particles decreases with the increase in depth [18, 19]. However, if two or more arrays of the rotors are to be installed at different depths, then the rotor diameter should match the orbital size at that particular depth (Fig. 1). Due to the orbital motion, there will always be a strong component of flow striking the concave surface of the blades. The diameter of the rotors should be less than the length of the rotor and the wave height [18]. The longer rotor gives more area of contact between the blades and the flow, and hence more momentum. The wave height determines the size of the orbit in all types of water waves [4, 20].

The present work is aimed at studying the energy extraction from the orbital motion of the particles by Savonius rotors. Most of the previous studies on ocean waves are performed either for designing ocean structures or focused on the common energy extraction devices such as Oscillating Water Column or Tapered Channel. In the present work, the characteristics of the waves are first studied and then a suitable rotor is designed and tested for energy extraction from the orbital motion of particles *only*. There is no reported work on the design and testing of such rotors, and this provided the motivation for this work.

2. Experimental set-up and procedure

The experiments were carried out in a *Cussons* Wave Channel model P6325 available in the Thermo-fluids laboratory of the University of the South Pacific. The wave channel had a length of 3500 mm, a width of 300 mm, and a depth of 450 mm. The side walls were made of Plexiglas to allow for a clear view of the wave action. A flap type wave maker hinged at the bottom produced sinusoidal waves with characteristics of deep water waves [21]. A frequency (f) range of 0 to 1.4 Hz was set. The close fit of the wave maker to the channel sides ensured that 2-D waves were produced with no fluid motion normal to the side walls [8, 21]. Fig. 2 shows a schematic diagram of the wave channel. The water flow was generated by a centrifugal pump having a rated capacity of 40 Lit/s at a total head of 10 m and driven by a 5.5 kW motor. The pump drew water from a tank with a 1.5 m × 0.8 m cross-section, which received the same water back from the wave channel. To minimize reflection of the waves, a *Cussons* Tuneable Beach model P6285 was installed at the end of the wave channel. It employed a series of porous plates with different porosity levels to absorb the wave energy gradually. The use of different plates with a variable spacing between them allowed for a wide variety of wave profiles to be absorbed.

The rotors had an outer diameter (d) of 66 mm, which is equal to the mean diameter of the orbits at the surface averaged over the frequency range investigated and is closest to that corresponding to 0.9 Hz. Each rotor had five blades made of galvanized iron sheets bent at 76º. Roller bearings were mounted at the shaft ends for a friction-free rotation. The ro-

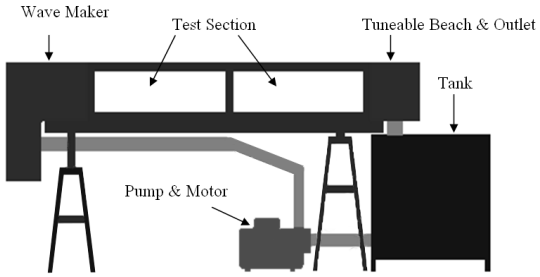

Fig. 2. Schematic diagram of the wave channel.

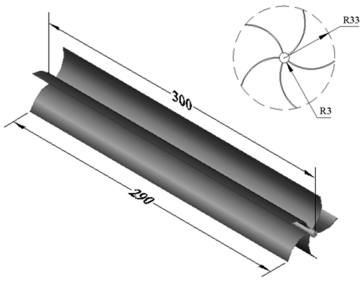

Fig. 3. Geometric details of the rotor (dimensions in mm).

tors were placed across the width of the wave channel and parallel to the wave front. The geometric details of the rotors are shown in Fig. 3.

The wave height and the wavelength were measured using *Seiki* pressure transducers model PSHF002KAAG. Data were acquired on a GL500A midi-LOGGER dual data logger, which was connected to the pressure transducers. The wave period was measured by recording the time it took for two successive crests to pass a given point. Wave frequency was calculated by taking the reciprocal of the wave period and by varying it from 0.58 to 1.1 Hz.

The Particle Image Velocimetry (PIV) system used in the present study was comprised of a 500 mW air-cooled Diode-Pumped Solid State continuous light laser and a high-speed *Photron* CCD camera. The 532 nm output of the laser was converted to a laser sheet and was delivered at the desired location. Poly Vinyl Chloride tracer particles, with an average diameter of 100 μm and a specific gravity of 1.02, were used for seeding the flow. The camera recorded 125 frames per second, producing up to 1280 x 1024 pixel images. The images captured by the CCD camera were processed using the Cactus 3.3 software. A schematic diagram of the PIV setup for the present work is shown in Fig. 4.

The wave parameters were varied by changing the frequency of the wave maker. The water depth was kept constant at 260 mm for all the experiments. The array of rotors was tested at four different submergence levels below the mean level. The center-to-center distance between the rotors was varied from 1.03 d to 2.0 d. The distance of the first rotor from the paddle was kept much greater than twice the depth of the hinge to ensure fully developed waves [21]. To ensure that the small reflections from the Tuneable Beach do not introduce measurement errors, a distance of at least one-and-a-half

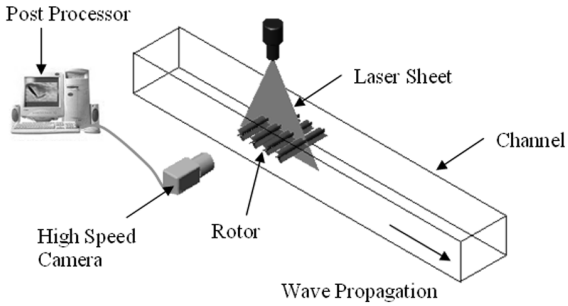

Fig. 4. Schematic of the PIV setup.

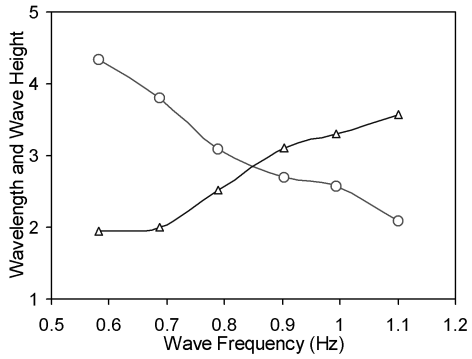

Fig. 5. Variations of the wavelength, λ/D (symbol ○), and wave height, 10H/D (symbol Δ) with frequency.

wavelengths was maintained between the last rotor and the Beach. The rotational speeds were recorded with a *Compact Instruments* optical tachometer model CT6LSR. The tachometer had an accuracy of 0.01% and a resolution of ±1 rpm.

The maximum error in the measurements of the rotational speed (rpm) of the rotors was estimated to be 3.33%. The factors considered for determining the accuracy of velocity measurements with PIV are the following: uncertainties due to finite time sampling, finite displacement of the particles, and uncertainties in measuring the displacements of the particle images [22]. The accuracy of the displacement measurements with *Cactus* is in the order of 0.1 pixels. For the high speed camera, the time resolution for the current measurements was 0.008 s. To obtain an accurate estimate of the uncertainty in our measurements, most of which were for rotating (orbital) motion of particles, PIV measurements were performed on a calibrated, constant speed rotating motion, and the maximum error was found to be 0.32%.

3. Results and discussion

Fig. 5 shows the variations of the wavelength and the wave height with frequency. The wavelength decreased with the increase in frequency, and it was high for larger wave periods. Higher wave period means fewer waveforms pass a given point. The wave height increased with the frequency of up to f = 0.9 Hz, after which it slowed, possibly due to the onset of wave breaking.

Detailed PIV measurements were performed to study the

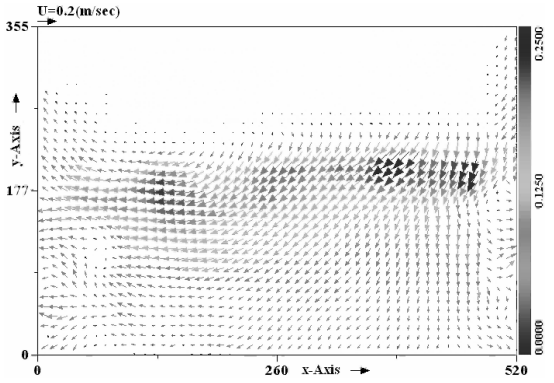

Fig. 6. Velocity vectors showing the left-downward motion of the particles in their orbital motion for the phase position of θ = 180°-270° at a frequency of 0.9 Hz.

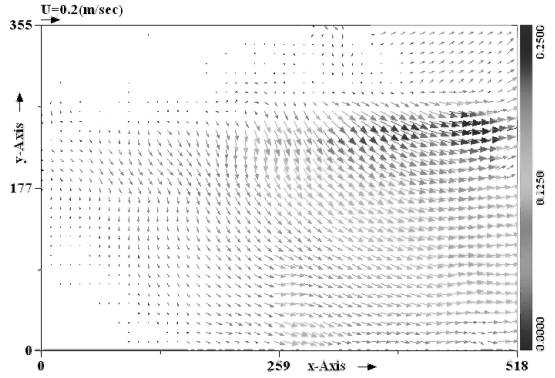

Fig. 7. Velocity vectors showing the right-downward motion of the particles in their orbital motion for the phase position of θ = 270-360° at a frequency of 0.9 Hz.

motion of the particles and gain a better understanding of the orbital motion at different wave frequencies. The velocity vectors at a frequency of 0.9 Hz at the same location but two instances corresponding to the phase positions θ = 180-270° and θ = 270-360° in the measurement area are shown in Figs. 6 and 7, respectively. The phase position θ = 0° refers to the wave crest. The velocities for the phase position θ = 180-270° are oriented in the up-wave direction, with the velocity vectors pointing left-downwards.

The predominantly horizontal movement of particles in the negative x-direction present under the trough can be seen on the left side of the measurement grid. The velocities for the phase position θ = 270-360° are oriented in the down-wave direction, with the velocity vectors pointing right downwards. The predominantly horizontal movement of particles in the positive x-direction present under the crest can be seen on the right side of the measurement grid. The trajectories of the particles can also be seen from the figures, and this is supported by theoretical analysis [4, 20]. These motions combine and result in the orbital motion as discussed earlier.

Fig. 8 shows the variation of the non-dimensional rotor rpm, N_n, averaged over the frequency range investigated and nearly equal to those at the frequency of 0.9 Hz. The center-to-center distance is between the rotors (c), which is normalized with the diameter of the rotor.

The rotational speeds of the rotors were normalized with those of the first rotor when the spacing between the rotors (c) was at the minimum (1.03 d). The submergence of the rotors was 1.21 d. The rotational speeds were found to decrease as the spacing increased, except for rotor R1 whose speed increased by about 10% from the minimum spacing to the maximum. The direction of rotation of all the rotors was clock-wise when the wave motion was in the x-direction. It is interesting to observe that the N_n of a particular rotor was always greater than its preceding rotor (except for c/d = 2 when the speeds of all the rotors were equal), which indicates that the preceding rotor directed the flow towards the blades of the next rotor located on top at that instant. Moreover, the rotors in the back experienced lesser drag due to their being in the

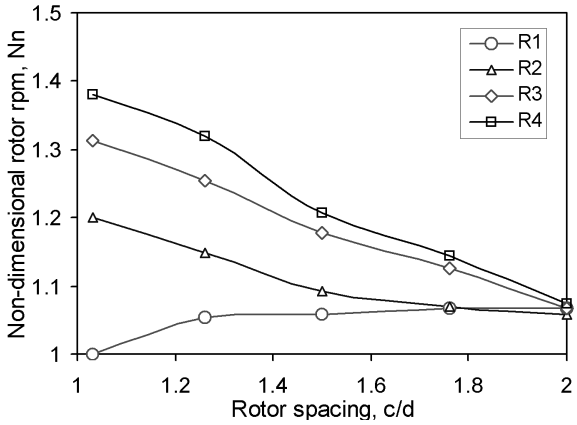

Fig. 8. Variation of the rotors' rpm, with the center-to-center distance between the rotors for z/d = -1.21.

wake of the front ones, which results in an increase in their rotational speeds.

The results of the PIV measurements for the case when the submergence of the rotors is *z/d* = -1.21 and the spacing is *c/d* = 1.03 are shown in Fig. 9. The phase position is θ = 0-90° for this case, with the crest approaching the measurement area. The rotors were very well-aligned to receive the energy of the orbiting particles, and their direction of rotation matched the orbital motion. When the wave crest approached the top of the rotors, there was a strong velocity component in the x-direction, which imparted considerable momentum to the blades that received that flow. Another interesting observation is that the flow exiting a front rotor could not exert a retarding force on the back rotor, as not much of the flow could penetrate the small spacing between the rotors. In the present experiments, it was possible to capture the flow around only three rotors due to the size of the measurement grid that was achievable with the available instrumentation.

When the rotor spacing increased, the energy of the particles in their orbital motion was not fully utilized by the rotors. The velocity vectors for higher values of *c/d* (not shown) indicate that the rotor blades receive lesser energy of the particles compared with the case when the rotors were close to each

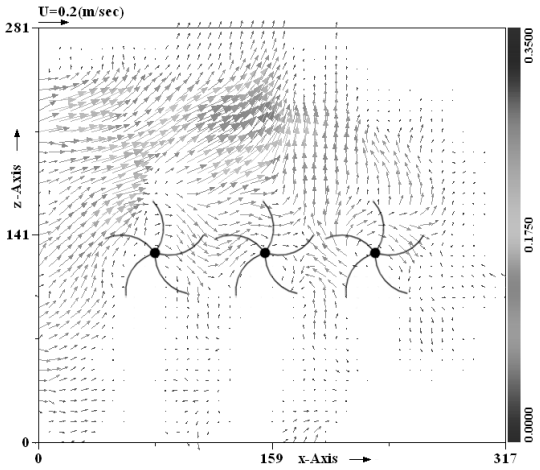

Fig. 9. Velocity vectors showing the interaction of the particles in their orbital motion with the first three rotors for the phase position of θ = 0-90° at a frequency of 0.9 Hz for rotor spacings of c/d = 1.03 and submergence of z/d = -1.21.

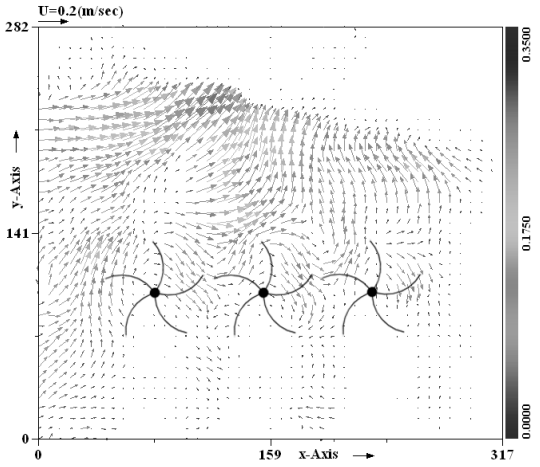

Fig. 10. Velocity vectors showing the interaction of the particles in their orbital motion with the first three rotors for the phase position of θ = 0-90° at a frequency of 0.9 Hz for rotor spacings of c/d = 1.03 and submergence of z/d = -1.52

other. At deeper submergence levels, the size of the orbits is reduced, which means that lesser momentum is imparted to the outer edges of the blades, as the rotor diameter will be larger than the size of the orbits at greater depths. Moreover, the kinetic energy of the orbiting particles is reduced with the increase in depth [18, 19], which contributes to a reduction in the speeds of the rotors. Fig. 10 shows the velocity vectors for the case when the submergence of the rotors is *z/d* = -1.52 and the spacing is *c/d* = 1.03 for the same phase position. The energy imparted to the blades is lesser compared with the case of lower submergence. A comparison of Figs. 9 and 10 shows that the major difference is in the kinetic energy received by the top portion of the rotors from the orbiting particles. At lower submergence, a much higher kinetic energy was available, which contributed to higher rotational speeds compared with the deeper submergence levels.

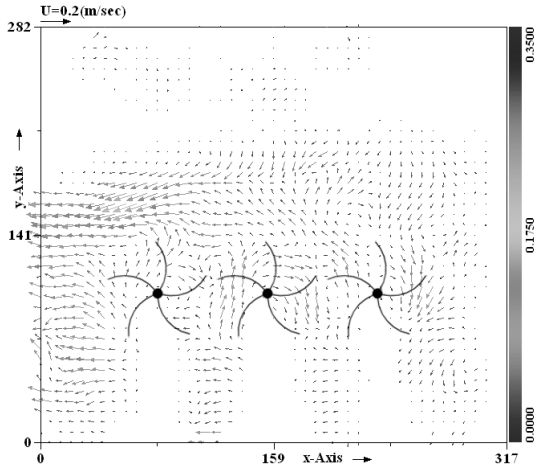

Fig. 11. Velocity vectors showing the interaction of the particles in their orbital motion with the first three rotors for the phase position of θ = 180-270° at a frequency of 0.9 Hz for rotor spacings of c/d = 1.03 and submergence of z/d = -1.52.

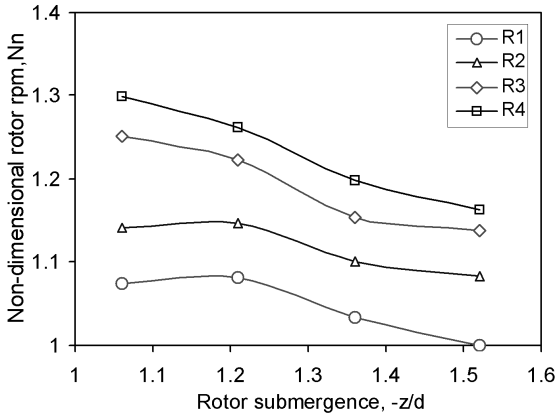

Fig. 12. Effect of submergence on the rotors' rpm.

The velocity vectors showing the interaction of the particles in their orbital motion with the first three rotors for the phase position of θ = 180-270° at a frequency of 0.9 Hz for rotor spacings of *c/d* = 1.03 and submergence of *z/d* = -1.52 are shown in Fig. 11. For this position, the direction of flow was also clearly well-aligned with the direction of rotation. The unique feature of these rotors is that compared with other water-driven turbines, mechanical energy is obtained by the momentum imparted to the blades on the curved surface. There is always a directional flow striking the concave surface of the blades. It is interesting to note that the pressure does not reduce anywhere during the energy transfer from the orbiting particles to the rotor, thus eliminating any risk of cavitation. Fig. 12 shows the variation in the speeds of the rotors averaged over the frequency range investigated (and nearly equal to the rotational speeds corresponding to the frequency of 0.9 Hz) with submergence. The higher rotational speeds were obtained close to the surface for the reasons discussed earlier. The orbital size and the wake of the front rotors appeared to have the strongest influence on the rotor R4, in which the drop

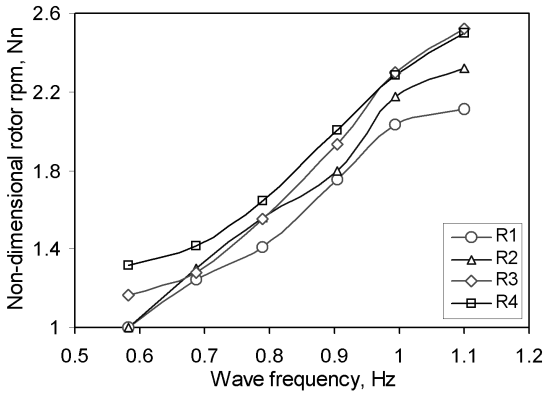

Fig. 13. Variation in the rotors' rpm with wave frequency.

in the rotational speed with deeper submergence was higher compared with the other rotors. In the present work, the power output of the rotors could not be measured with reasonable accuracy due to the light weight of the rotors, which did not respond well to a practical load that could be measured accurately. Nevertheless, it is expected that at low damping coefficients, the behavior of the rotors will not be significantly different from the undamped case [23-25]. The power output is expected to peak at a particular frequency in the case of harmonic waves. However, in the case of ocean waves, the peak may not be pronounced at a particular frequency due to the broad distribution of frequencies [24].

The variation in rotational speeds of the rotors with wave frequency is shown in Fig. 13. At lower frequencies, the wave height was less (shown in Fig. 5), hence the available wave energy was also less, as discussed earlier. The wave height increased with the frequency, thus increasing the wave energy and the speeds of the rotors. However, wave height is known to increase with the frequency up to a certain steepness ($H/\lambda \cong 0.13$), beyond which wave breaking occurs, causing a reduction in the wave height, available wave energy, and speeds of the rotors. The results of the present work offer an innovative method of generating power from ocean waves. Based on the results, employing a large number of rotors in an array is clearly advantageous. It can be concluded from the results in Figs. 8 and 12 that if more rotors are employed, their rotational speeds will be higher than these rotors, enabling more energy to be harnessed. There can also be a number of such arrays at different depths, with the diameters of rotors decreasing with the increasing depth to match the size of orbits.

4. Conclusions

The orbital motion present in underwater waves was first investigated and then utilized to drive an array of four Savonius rotors. The highest rotational speeds of the rotors were recorded close to the water surface, where the maximum energy was available due to the largest size of the orbits. The speeds of the rotors decreased with the increase in spacing between the rotors. At lower frequencies, the wave height was found to be lower, which means that there was less available energy. The rotational speeds of the rotors increased rapidly up to a certain frequency, after which the wave started breaking. A directional flow always striking the concave surface of the blades was observed. It is interesting to note that the pressure does not reduce anywhere during the energy transfer from the orbiting particles to the rotor, thus eliminating any risk of cavitation.

Nomenclature

c	:	Center-to-center distance between the rotors, m
d	:	Outer diameter of Savonius rotor, m
D	:	Water depth, m
F	:	Wave frequency, Hz
H	:	Wave height, m
N_n	:	Non-dimensioned rotor rpm
x	:	Streamwise coordinate, m
y	:	Transverse coordinate, m
z	:	Vertical coordinate, m
λ	:	Wavelength, m
θ	:	Phase position, degree

References

[1] P. Janssen, *The interaction of ocean waves and wind*, first ed., Cambridge University Press, UK, (2004).

[2] J. Falnes, A review of wave-energy extraction, *Marine Structures*, 20 (4) (2007) 185-201.

[3] M. E. McCormick, *Ocean wave energy conversion*, first ed., Dover Publications, New York, USA, (2007).

[4] L. H. Holthuijsen, *Waves in oceanic and coastal waters,* first ed., Cambridge University Press, UK, (2007).

[5] K. A. Sverdrup, A. B. Duxbury and A. C. Duxbury, *Fundamentals of oceanography*, fifth ed., McGraw Hill, New York, USA, (2006).

[6] B. L. Mehaute, *An Introduction to Hydrodynamics and Water Waves*, first ed., Springer-Verlag, New York, USA, (1976).

[7] K. U. Graw and J. Lengricht, Comparison of LDV and ultrasonic measurement of orbital velocity, *Proceedings of XXV IAHR Congress,* Tokyo, Japan, (1993) 81-88.

[8] C. Gray and C. A. Greated, The application of particle image velocimetry to the study of water waves, *Optics and Lasers in Engineering*, 9 (3-4) (1988) 265-276.

[9] D. Stagonas and G. Müller, Wave field mapping with particle image velocimetry, *Ocean Engineering*, 34 (11-12) (2007) 1781-1785.

[10] A. Constantin, On the deep water wave motion, J. Phys. A: Math. Gen. 34 (7) (2001) 1405-1417.

[11] J. Pedlosky, *Waves in the Ocean and Atmosphere: Introduction to Wave Dynamics*, first ed., Springer-Verlag, Berlin Heidelberg, Germany, (2003).

[12] J. Twidell and A. D. Weir, *Renewable Energy Resources*, second ed., Taylor and Francis, New York, USA, (2006).

[13] R. Pelc and R. M. Fujita, Renewable energy from the ocean,

Marine Policy, 26 (6) (2002) 471-479.

[14] J. L. Menet, A double step Savonius rotor for local production of electricity: a design study, *Renewable Energy*, 29 (11) (2004) 1843-1862.

[15] P. Reupke and S. D. Probert, Slatted-blade Savonius windrotors, *Applied Energy*, 40 (1) (1991) 65-75.

[16] M. N. I. Khan, M. T. Iqbal and M. Hinchey, *Sea-Floor Power Generation System*, available online at http://necec.engr.mun.ca/ocs2007/viewpaper.php?id=11&print=1.

[17] M. F. Merriam, Wind, waves, and tides, *Annual review of energy*, 3 (1978) 29-56.

[18] G. Jobb, *An ocean wave energy converter*, available online at http://www.treefinder.de/Ideas/WaveConverter.pdf.

[19] H. K. Chang, J. C. Liou and M. Y. Su, Particle trajectory and mass transport of finite-amplitude waves in water of uniform depth, *European journal of mechanics - B/Fluids*, 26 (3) (2007) 385-403.

[20] M. Rahman, *Water waves - Relating modern theory to advanced engineering practice*, first ed., Oxford University Press, New York, USA, (1994).

[21] M. Rea, Wave tank and wavemaker design, in *Ocean wave energy – current status and future perspectives*, ed. João Cruz, Springer-Verlag, Berlin Heidelberg, Germany, (2008) 147-159.

[22] M. Raffel, C. Willert and J. Kompenhans, *Particle Image Velocimetry – A Practical guide*, first ed., Springer, Berlin Heidelberg, Germany, (1998) 105-166.

[23] P. M. Coola, M. Ravindran and P. A. A. Narayana, Model studies of oscillating water column wave-energy device, *ASCE J. Energy Engineering*, 121 (1994) 14-26.

[24] M. Eriksson, J. Isberg and M. Leijon, Hydrodynamic modelling of a direct drive wave energy converter, *Int. J. Engg. Sci.*, 43 (2005) 1377-1387.

[25] B. F. M. Child and V. Venugopal, Interaction of waves with an array of floating wave energy devices, Paper No. 1059, *Proceedings of the 7th European Wave and Tidal Energy Conference,* Protugal, (2007).

M. Rafiuddin Ahmed obtained his Ph.D. degree in Thermo-fluids Engineering from the Indian Institute of Technology (IIT) Bombay, India, in 1998. He is currently the Head of the Division of Mechanical Engineering at the University of the South Pacific, Suva, Fiji.

Young-Ho Lee obtained his Ph.D. degree from the Department of Mechanical Engineering, University of Tokyo, Japan, in 1992. Currently, he is a Professor in the Division of Mechanical Engineering at the Korea Maritime University. He is the vice president of Korea Wind Energy Association and Korea Fluid Machinery Association.